RESEARCH ARTICLE

E. Lagios · V. Sakkas · Is. Parcharidis · V. Dietrich

Ground deformation of Nisyros Volcano (Greece) for the period 1995–2002: Results from DInSAR and DGPS observations

Abstract Differential GPS (DGPS) and Differential Interferometric Synthetic Aperture Radar (DInSAR) analyses were applied to the Kos-Yali-Nisyros Volcanic Field (SE Hellenic Volcanic Arc) to quantify the ground deformation of Nisyros Volcano. After intense seismic activity in 1996, a GPS network was installed in June 1997 and re-occupied annually up to 2002. A general uplift ranging from 14 to 140 mm was determined at all stations of the network. The corresponding horizontal displacements ranged from 13 to 53 mm. The displacement vectors indicate that the island is undergoing extension towards the East, West and South. A two-source "Mogi" model combined with assumed motion along the Mandraki Fault was constructed to fit the observed deformation. The best-fit model assumes sources at a depth of 5500 m NW of the centre of the island and at 6500 m offshore ESE of Yali Island. DInSAR analysis using four pairs of images taken between May 1995 and September 2000 suggests that deformation was occurring during 1995 before the start of the seismic crisis. An amplitude of at least 56 mm along the slant range appeared for the period 1996 through 1999. This deformation is consistent with the two-source model invoked in DGPS modelling. Surface evidence of ground deformation is expressed in the contemporaneous reactivation of the Mandraki Fault.

E. Lagios (✉) · V. Sakkas · I. Parcharidis
Space Applications Research Unit in Geosciences, Laboratory of Geophysics, Department of Geophysics & Geothermics, National Kapodistrian University of Athens, Panepistimiopolis-Ilissia, 157 84 Athens, Greece
e-mail: lagios@geol.uoa.gr

V. Dietrich
Swiss Federal Institute of Technology, Institute of Mineralogy and Petrography, ETH-Zentrum, CH-8092 Zurich, Switzerland

Present address:
I. Parcharidis
Department of Geography, Harokopio University, Athens, Greece

In addition, a 600 m long N-S trending irregular rupture in the caldera floor was formed between 2001 and 2002. This rupture is interpreted as the release of surface stress in the consolidated epiclastic and hydrothermal sediments of the caldera floor.

Keywords Nisyros volcano · Ground deformation · SAR Interferometry · DGPS measurements · Mogi model · IKONOS imagery · Hellenic Volcanic Arc.

Introduction

Nisyros Island is part of the Kos-Yali-Nisyros Volcanic Field in the SE part of the Aegean Sea (Fig. 1). Intense seismic activity started in the broader area of Nisyros at the beginning of 1996 and lasted through the end of 1998. Differential GPS (DGPS) and Differential Interferometric Synthetic Aperture Radar (DInSAR) analyses have proven to be powerful tools for the monitoring of small surface changes over large-scale areas (Zebker and Goldstein 1986; Dixon 1991; Sigmundsson et al. 1992) and have been used in this study to quantify the deformation associated with the recent (1996–1998) seismic crises. In this paper, we present the results of DGPS and DInSAR analyses as compared to simple elastic modelling of two point sources. First, we briefly summarize the tectonic and structural setting of Nisyros volcano and its associated hydrothermal field, as well as the recent seismic crises.

The geotectonic setting of the Kos-Yali-Nisyros volcanic field

The Hellenic Volcanic Arc is a magmatic expression of the active northeastward-directed subduction of the African Plate beneath the Aegean Plate, which started around 5 Ma at the beginning of Pliocene (McKenzie 1972; Le Pichon and Angelier 1979; Papanikolaou 1993; Jackson 1994). The base of the volcanic arc rests on normal and thinned
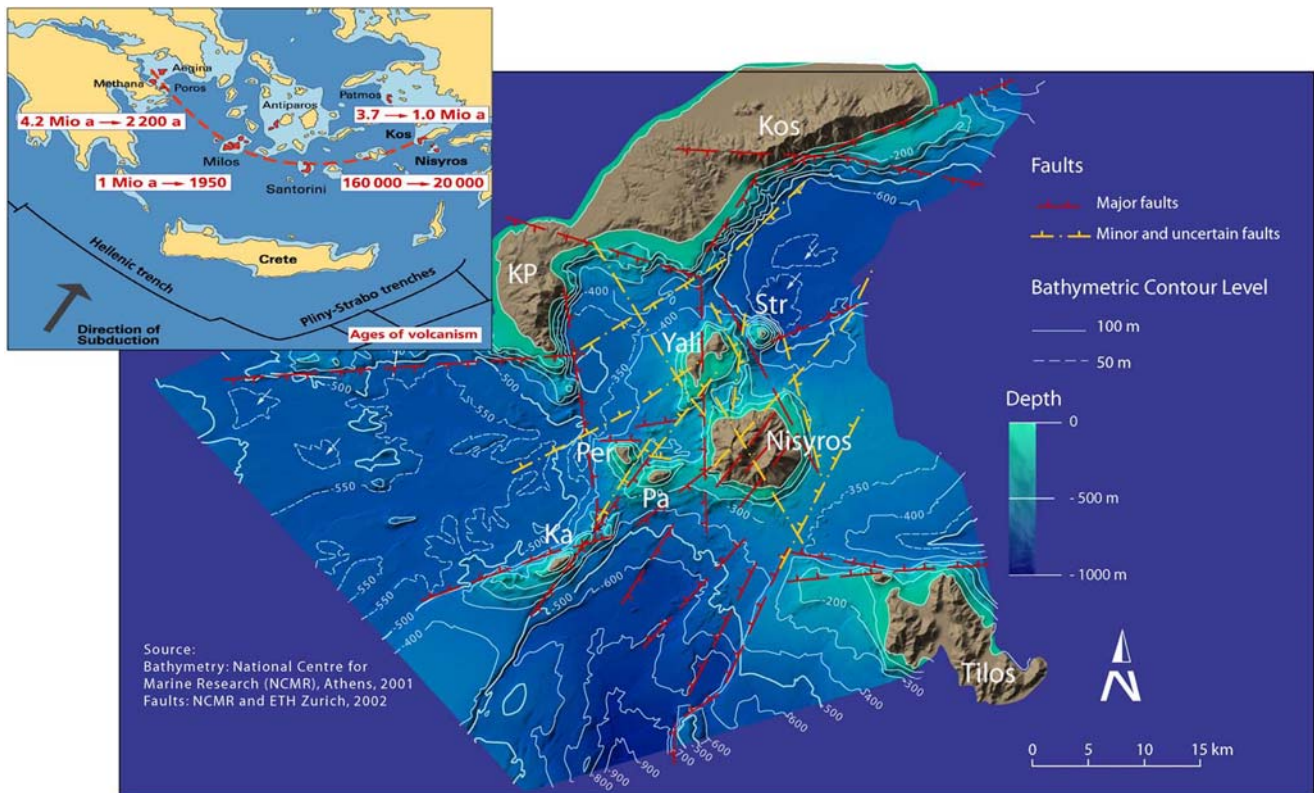
Fig. 1 The Hellenic Volcanic Arc showing the main volcanic centers. Bathymetry and topography of study area of Kos-Yali-Nisyros volcanic field. Abbreviations: *KP*: Kephalos Peninsula, *Str*: Strongili, *Per*: Pergussa, *Pa*: Pachia, *Ka*: Kandelussa

continental crust that has undergone several stages of deformation and metamorphism during the Alpine Orogeny from Cretaceous to late Tertiary (Smith 1971).

The eastern sector of the Hellenic Volcanic Arc, including the islands of Kos, Yali and Nisyros, comprises the largest volumes of volcanic materials. Although the Dodecanese Islands, the Bodrum Peninsula and Kos have been affected by magmatic and volcanic activity over the past 10 million years (Fytikas et al. 1976, 1984; Pe-Piper and Piper 2002), high geodynamic activity in the Kos-Yali-Nisyros Volcanic Field started in the Pliocene (approx. 2.6–2.8 my) with phreato-magmatic eruption of ignimbrites. Large remnants of these eruptives phases are present in the Kephalos Peninsula (Kos) and in the islets of Pergussa and Pachia (Fig. 1).

Approximately 160,000 years ago, ignimbrites were emplaced in the region of the NE-striking "Kos Horst-Graben System" in the largest eruption in the Eastern Mediterranean, emitting more than 100 km³ of pyroclastic material (Kos Plateau Tuff). Ash, pumice and pyroclastic flows devastated an area of more than 3000 km² (Keller 1969; Smith et al. 1996; Allen et al. 1999). The center of this catastrophic eruption was probably located N to NE of Yali (Fig. 1). As a result, a present-day submarine caldera with a diameter of 15–20 km was formed, which is now covered up to several kilometers with volcano-sedimentary materials from younger eruptions. Since 140,000 years ago the volcanic edifices of Nisyros, Yali and Strongyli (Fig. 1) have grown

on the central part and rim of this caldera (Papanikolaou et al. 1991; Vougioukalakis 1993).

Nisyros Volcano—Structural setting

Nisyros Island, resembling a pentagon in shape, has an average width of about 8 km and covers an area of about 42 km² (Fig. 2). It lies above a basement of Mesozoic limestone (Geothermica Italiana 1983; 1984) and a thinned crust, with the Moho located at a depth of about 27 km (Makris and Stobbe 1984). The exposed rocks are Quaternary volcanics. The evolution of Nisyros Volcano during the past 160,000 years, together with the succession of calc-alkaline lavas and pyroclastic rocks, has been studied in detail by various authors (Di Paola 1974; Keller et al. 1990; Papanikolaou et al. 1991; Limburg and Varekamp 1991; Vougioukalakis 1993; Hardimann 1999).

Five major fault systems have been identified within the volcanic edifices of the Kos-Yali-Nisyros Volcanic Field (Figs. 1 and 2) on the basis of recent structural and geological investigations (Papanikolaou et al. 1991; Vougioukalakis 1993; Papanikolaou and Nomikou 2001).

The F1 (NE-SW) fault system: The F1 fault system trends NE-SW and is part of the large horst-graben system between the islands of Kondeliousa, Kos and the Datça Peninsula. A down-faulting of several hundred meters of the central parts must have occurred since early Pleistocene

Fig. 2 Fault pattern, location of hydrothermal explosion craters and hot springs superimposed on a digital elevation model (DEM) of Nisyros Island, derived by digitizing the 1:5000 scale topographic map sheets of Nisyros Island, 1983 (published by the Hellenic Military Geographical Service, Greece). Abbreviations of locations: *Av*: Avlaki, *Af*: Afionas, *CA*: Cape Akrotiri, *CK*: Cape Katsuni, *AI*: Agia Irini, *Le*: Lephkos, *Lo*: Loutra, *LP*: Lakki Plain, *LR*: Lakki Rupture, *Ma*: Mandraki, *ME*: Monastery Evangelistra, *N*: Nikia, *Pa*: Pali, *PE*: Prophitis Elias, *PK*: Monastery Panagia Kyra, *Th*: Thermiani
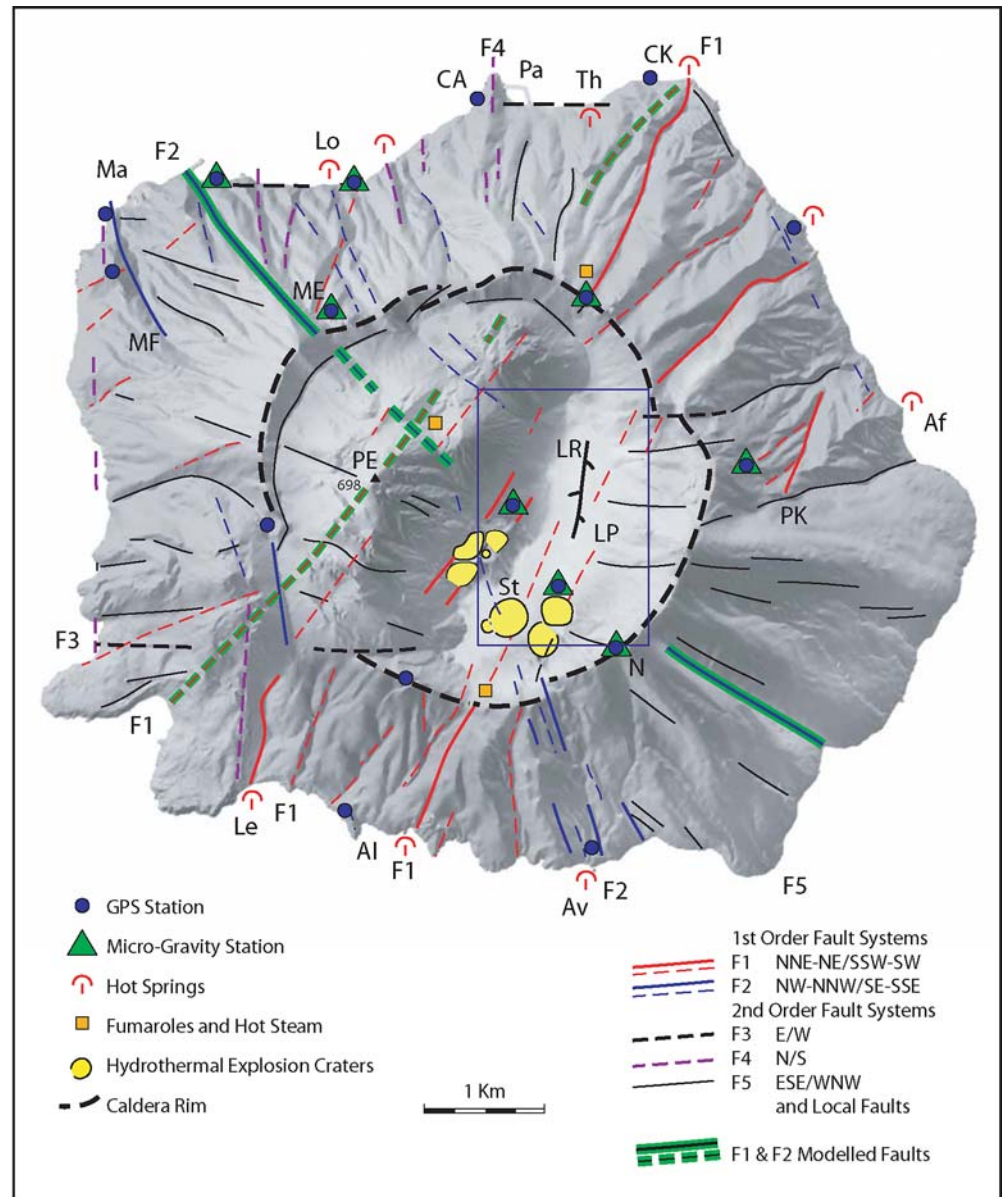
(Geological Maps of Kos Island: Sheet Kephalos (Triantaphyllis 1994) and Kos (Triantaphyllis and Mavrides 1998)). A series of F1 faults crosscut the entire island of Nisyros along the borders of the Lakki Plain and has caused down-faulting of the western part of the Agia Irini block (Fig. 2) in the south. All hydrothermal explosion craters are located at the intersections between the conjugate fault system F1 and F2. At the northern and southern extensions of the F1 system, hot springs occur at sea level (Cape Katsuni and Thermiani in the north, and Lefkos in the south).

The F2 (NW-SE) Fault System: These faults run more or less perpendicular to the F1 fault system and have steep inclinations of 70° to 80° at the surface but with dips changing between NE and NW. Characteristics of this fault system are extensional features and down-faulting with displacements up to 70 m. It extends from the NW part of Tilos Island into Nisyros Island in the area of Avlaki, crosscuts

the entire island, runs along the western part of Yali and merges into Kos Island. A series of NW-SE parallel faults cut Nisyros Island in the area of Avlaki and Agia Irini blocks (Fig. 2). Best evidence for down-faulting of the latter is noted from the offset of the southern caldera rim. The fault system runs through the hydrothermal eruption craters (Brombach et al. 2001, 2003).

The F3 (E-W) Fault System: The localized F3 fault system is oriented E-W and might be the result of the deep reaching conjugate F1 and F2 fault systems. Surface expressions are visible along the northern coast of Nisyros at the town of Mandraki, between the harbours at Mandraki and Loutra, between Pali and Cape Katsuni, as well as in the Karaviotis lava flows bordering the Kateros cove and in the western slopes of the monastery Panagia Kyra. The hot spring of Afionas at sea level might also be a result of this fault system. Similar E-W striking faults occur in the Neogene

sediments and the Pleistocene Kos Plateau Tuff in Kos Island.

The F4 (N-S) Fault System: A subordinate N-S trending fault system can be locally identified in the volcanic edifice of Nisyros Island along the northwestern coast between the dacitic domes of Karaviotis and Trapezina and at Cape Akrotiri. Based on bathymetry, the latter fault appears to extend into a small N-S graben between Yali and Strongyli. An equivalent fault system seems also to be present in the Kephalos Peninsula at Kos Island. Similar to the F3 system, the F4 system might also be a result of the dominant conjugate F1 and F2 systems.
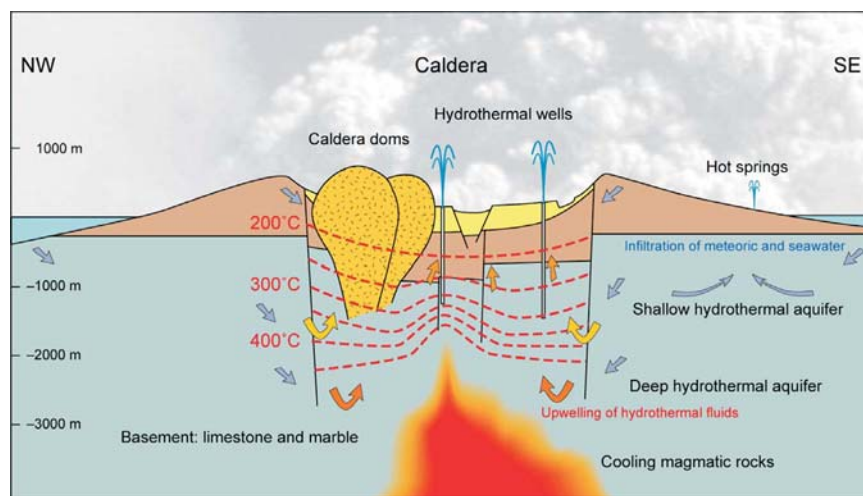
The F5 (ESE-WNW) Fault System: These faults are observed in the older volcanic series, as well as in the youngest volcanic intrusives inside the caldera, and must be related to a regional fault system along which down-faulting of major blocks in Kos took place.

The Caldera Rim: The caldera rim and its accompanying cone-shaped local faults are entirely volcanic structures, which are a result of the caldera collapse after the last Plinian eruptions. Neither displacement nor hydrothermal activity has been recognised within the rim and these local faults.

Hydrothermal system

Although the last magmatic activity on Nisyros dates back to at least 15,000 years, volcanic unrest as expressed by seismic activity is continuously present. Such activity is reported since historical times and is partially a result of the hydrothermal system at crustal levels less than 1,500 m (Dawes and Lagios 1991). This system (Fig. 3) is expressed by brine temperatures above 300°C at 1,700 m depth. Its surface expressions are fumaroles and hydrothermal explosion craters within the caldera, as well as several thermal springs with temperatures between 30 and 60°C that occur around the island (Fig. 2). During the latest hydrothermal explosion in 1873, fire and gas emanations were reported along the coast near the town of Mandraki (Gorceix 1873a, b, c).

Two distinct hydrothermal aquifers (Dawes and Lagios 1991) may be present underneath the caldera based on temperature distribution, fluid geochemistry, physical-chemical characteristics of the fumarolic gases and the thermal waters at the surface, as well as the waters in deep geothermal drill holes (Geothermica Italiana 1983, 1984). The deeper hydrothermal aquifer is characterized by high temperatures above 300°C and fluids of high salinity, whereas the shallow aquifer has temperatures around 100°C and boiling fluids with high concentrations of CH_4, CO_2, H_2 and H_2S gases (Chiodini et al. 1993; Marini et al. 1993; Kavouridis et al. 1999; Chiodini et al. 2002).

Seismic activity

Earthquakes have been described throughout historical times and reported in detail in 1830, 1871–73, 1887, 1953, 1961 and 1968–71 (Gorceix 1873a, b, c; Makropoulos et al. 1989; Stiros and Vougioukalakis 1996). Their origin may be a result of regional tectonic processes, magma ascent, degassing phenomena of deep crustal magma and steam explosions within the hydrothermal system as recognized by "hydrothermal noise".

Detailed accounts of the most recent seismic crisis which started in the beginning of 1996, culminated in 1997, continued through 1998, and returned to the background level at the beginning of 1999 are given by Papadopoulos et al. (1998), Makris and Chonia (1999) and Sachpazi et al. (2002). More than 1600 events generally striking NW-SE were located within the Kos-Nisyros-Tilos area. Most occurred at shallow depths with M_L magnitudes ranging from 1.2 to 3.2 over a period of only 3.5 months (Makris and Chonia 1999). Also, several shallow tectonic earthquakes at depths up to 10 km with larger magnitudes up to 5.5 occurred along the fault system between Tilos and Kos (Fig. 1). The Mandraki Fault (a branch of F2 fault system) was reactivated in 1996 and caused damage to buildings and other structures within the town of Mandraki (Ioannidis 1998). An associated increase of fumarolic activity was

Fig. 3 A schematic cross-section of Nisyros Caldera and the underlying hydrothermal system. The model is used to show the crustal and lithospheric structure of Nisyros volcanic island. Today the maximum height of the volcano is 698 m (Prophitis Elias) above sea level. The volcanic base in 300 m depth lies on top of Mesozoic limestone (Malm formation), which has been sampled during drilling of the two geothermal wells in the Lakki Plain in 1983 and 1984

noted along the western edge of the hydrothermal crater field (Brombach et al. 2001). Tectonic processes recently expressed by seismicity indicate tensional fracturing which could reduce the lithostatic pressure and trigger explosive volcanic phenomena such as those reported in 1871 and 1873 (Makris and Chonia 1999).

DGPS analysis

A geodetic GPS network (Fig. 2) consisting of 18 stations was established in the broader area of Nisyros Island in June 1997 and included a reference station in the NE part of Kos Island (Lagios et al. 1998; Lagios 2000). Stations were installed by emplacing benchmarks (bronze pins having head-diameter of 2.5 cm) on the ground surface of volcanic rock formations. However, in the absence of bedrock a few stations were established on the concrete surface of old constructions. The network was re-occupied in September 1997, May and October 1998, June 1999, July 2000, June 2001 and July 2002.

All DGPS measurements were made in the static mode using tripods above the benchmarks. Geodetic, dual-frequency WILD receivers (SR299 and SR399) were employed for all measurements. A local base-station was established in Mandraki that operated during the entire measurement period. Three other receivers were used as rovers and recorded for 4–5 h at a given station with a sampling interval of 15 s. Most of the stations were occupied more than once. Since the dimensions of the network are relatively small, the lengths of the measured baselines between the stations are small (3–4 km). The longest baseline is the one between the local base-station and the reference station on Kos (23 km), which was continuously measured for about 30 h with a 30 s sampling interval.

The Static Kinematic Software (SKI Pro 1999) of Leica allowed the *in situ* processing and adjustment of the GPS measurements. Post-processing was performed using the *Bernese GPS Software Version 4.2* (Rothacher et al. 1993), together with post-computed satellite orbits (available through the International GPS Service) to improve the error estimation. An accuracy of 2 to 3 mm in the horizontal component and 4 to 6 mm in the vertical was achieved. The adjusted results of all campaigns are presented in Fig. 4. This shows the overall deformation observed in Nisyros relative to the first measuring period (June 1997).

A consecutive annual analysis of the GPS data during the entire period of observation provides a temporal history of the ground deformation (Fig. 5). The maximum horizontal displacement occurred between 1997 and 1998 (Fig. 5a, b) during the peaking (1997) and subsequent high level (1998) of seismic activity (Sachpazi et al. 2002). The amplitude of the horizontal deformation ranged from 20 to 60 mm. In the following two periods (1998–1999 and 1999–2000), the amplitude decreased to 10 to 20 mm (Fig. 5c) and about 10 mm (Fig. 5d), respectively. However, the deformation increased again to about 15 mm at some stations
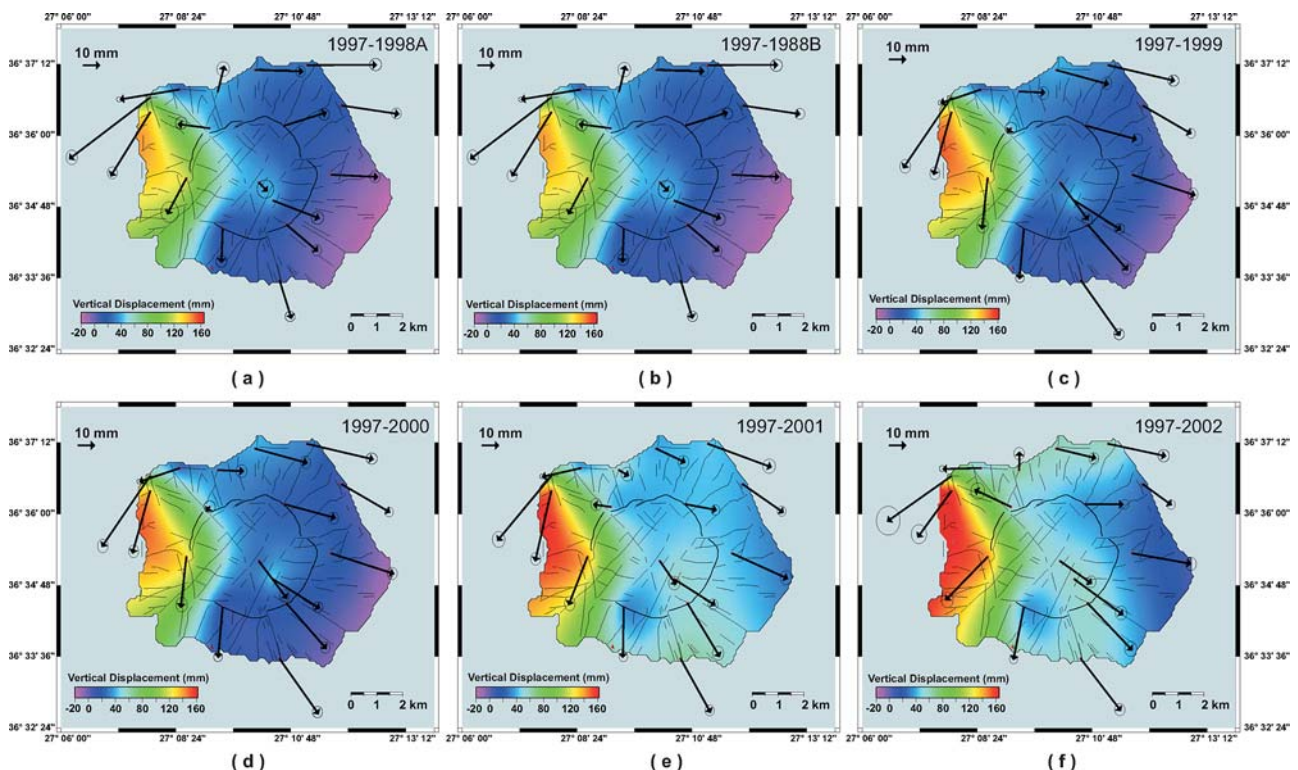
Fig. 4 DGPS horizontal and vertical displacements for the periods: (**a**) June 1997 – May 1998, (**b**) June 1997 – Oct. 1998, (**c**) June 1997 – Sept. 1999, (**d**) June 1997 – Sept. 2000, (**e**) June 1997 – June 2001 and (**f**) June 1997 – July 2002. The horizontal deformation is represented by arrows and the vertical displacement by colour contouring
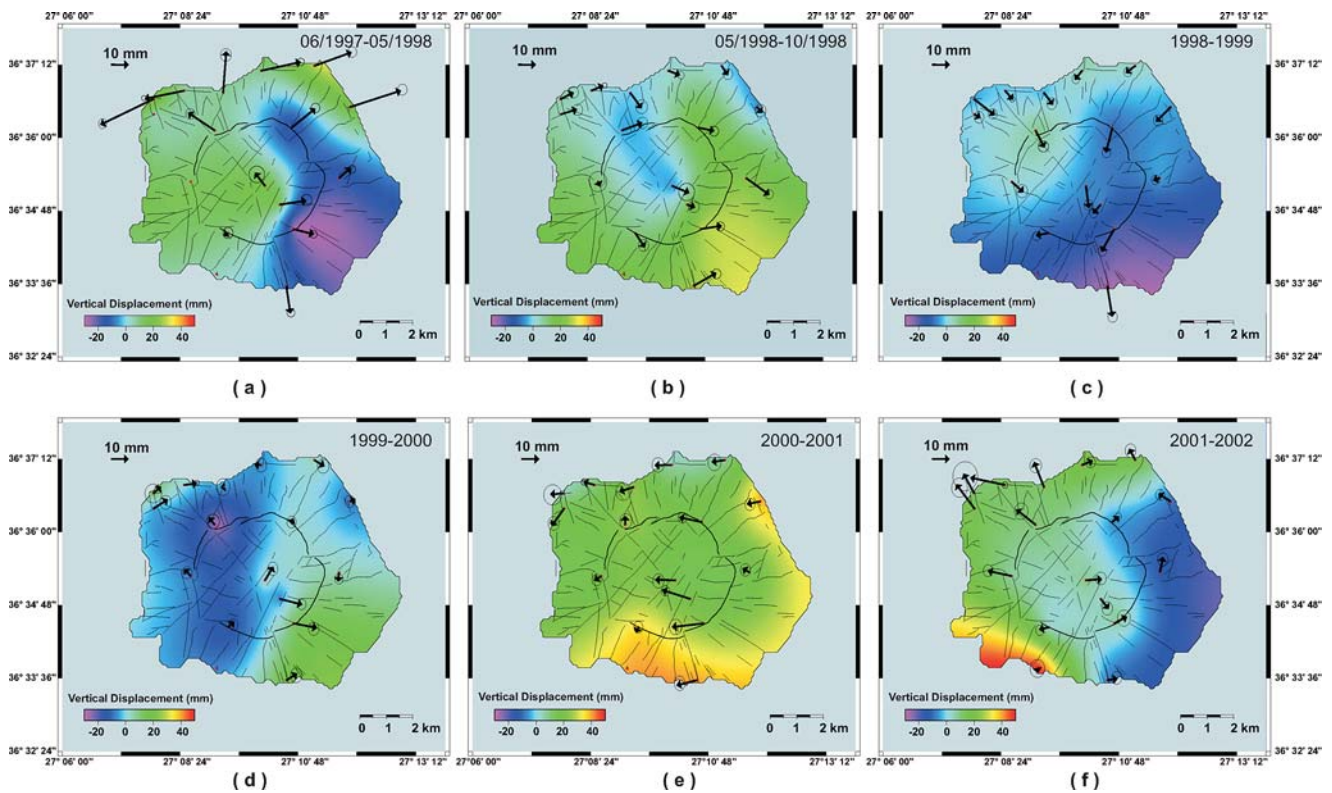
Fig. 5 DGPS results for individual measurement campaigns: 1997–1998 (**a**, **b**), 1998–1999 (**c**), 1999–2000 (**d**), 2000–2001 (**e**) and 2001–2002 (**f**). Legend as in Fig. 4

for the subsequent period (2000–2001; Fig. 5e). Finally, in the last period (2001–2002; Fig. 5f), Nisyros entered a different mode of deformation with a clear westward increase of the horizontal component in almost all its western part.

Vertical deformation in the sense of a general uplift of the whole island occurred over the entire period of observation. Except for three stations located on the uplifted side of the reactivated fault at Mandraki, where the vertical displacements reached values of 60 to 140 mm, the majority of stations recorded uplifts between 40 to 60 mm between 1997 and 1998. In the following periods, general uplift continued by only 8 mm (1998 to 1999), followed by a deflation of 15 mm (1999–2000) and further uplift of about 10 mm (2000–2001). For the last period (2001–2002), an uplift of about 10 mm occurred in the western, central and northern parts of the island, while the eastern area subsided by 10 mm.

For the entire monitoring period (1997–2002), the total displacements ranged from 10 to 60 mm and 30 to 150 mm for the horizontal and vertical components, respectively (Fig. 4). It appears that the island is undergoing extension almost along the two major faulting zones F1 and F2 (Fig. 2) to the West, East and South. After 1998 the horizontal displacement recorded at the NW and NE part of the island slightly changed directions from SW and ESE to SSW and SE, respectively.

Source interpretation

There are two plausible interpretations to explain the deformation observed by GPS. The first scenario involves fault motions along the major F1 and F2 fault zones. The second considers the inflation/deflation of magma chambers in the near vicinity of the area.

It may seem that the net observed deformation (Fig. 4f) is apparently controlled by the F1 and F2 fault systems that extend the island to the East, West and South. In support of this contention, the oldest rocks are exposed in an uplifted block in the NW part of the island (Stiros 2000). However, modelling attempts (to be discussed later) are not fully consistent with that interpretation.

Alternatively, there are several lines of evidence to support the existence of two magma chambers in the area. On the basis of geochemical evidence, increased H_2S/CO_2 ratios and decreasing CH_4/CO_2 ratios were determined to be caused by an increased contribution of the magmatic component to the recharge of the local hydrothermal system (Brombach et al. 2001). In addition, the largest magmatic inputs seem to occur below the main hydrothermal craters in the Lakki Plain (Chiodini et al. 2002; Brombach et al. 2003).

Geophysical evidence based on Audio-Magnetotelluric (AMT) measurements in the Nisyros high enthalpy geothermal field (Lagios 1991; Dawes and Lagios 1991) indicates

two conductive bodies beneath about the center of the island. These bodies merge into a single larger one at greater depths. This deep-seated body—inferred by the major axes of the MT polarisation ellipses in the frequency range of 0.1 to 0.01 Hz and interpreted as a magma chamber—is situated almost on the junction of the two main fault zones F1 and F2 at about the center of the island at a depth of about 6 to 9 km.

Geophysical evidence also favours the existence of a second suspected magma chamber located offshore. Detailed seismological analysis from a local temporary seismological network (Sachpazi et al. 2002) suggests the presence of an aseismic area just south of Yali (approximately 5 km north of Nisyros), which was interpreted as a low-strength/cohesion volume consistent with the location of a magma chamber. Existence of a volcanic intrusion in the same area that might have extruded from a larger magma volume located to the south is also supported by active seismic investigations in the broader area (Makris and Chonia 1999). The off-shore suspected magma chamber coincides with intersection of major sub-marine fault zones (Fig. 1).

Source modelling

Forward modelling was performed in an attempt to resolve the more likely scenario to explain the observed deformation. Assuming hypothetical fault activation along fault zones F1 and F2, displacements were quantified using the single plane fault algorithm of Feigl and Dupre (1999), which is based on the formulation of fault-dislocation developed by Okada (1985). Modelling parameters referring to likely minimum and maximum values of depth and length extent of the F1 and F2 faults were assumed (Table 1). An acceptable fit for the NW uplifted part was possible only for the vertical component of deformation. In this case, the values of the slip-component vector (U1,U2,U3) are relatively large. However, the horizontal fit displacements are unacceptable for both directions and amplitudes for almost all control points. On the other hand, when trying to fit the horizontal displacements for control points near the faults, a total misfit in both amplitude and direction resulted for the distant stations, whilst at the same time unacceptably large vertical deviations resulted at all control points. Thus fault activation cannot fully account for the observed ground deformation.

Additional modelling was performed to determine if pressure changes in high-level magma chambers could account for the observed deformation. A "Mogi model" (Mogi 1958) was adopted which assumes a small volume sphere of varying pressure, considered as a point source within an elastic half-space (where Poisson's ratio = 0.25), such that the elastic Lamé coefficients λ and μ are equal. The resultant deformation on the ground surface is radially symmetric and the horizontal radial displacement, Δr, and the vertical displacement, Δz, are respectively given by (cylindrical polar coordinates):

$$\Delta r = C \cdot r/(d^2 + r^2)^{3/2} \tag{1}$$

$$\Delta z = C \cdot d/(d^2 + r^2)^{3/2} \tag{2}$$

where d is the source depth, r the horizontal distance from the source, and C is the so called *source strength parameter* (Sigmundsson 1995) given by:

$$C = 3R^3(\Delta P)/4\mu \tag{3}$$

where ΔP is the pressure change within the sphere, R is the radius of the sphere, and μ is the rigidity of the crust surrounding the sphere. Equation (3) may also be presented as a function of volume change (ΔV) at depth (McTigue 1987):

$$(\Delta V)/\pi = R^3(\Delta P)/\mu \tag{4}$$

The period 1997 to 2001 was chosen for modelling (Fig. 4e), prior to the occurrence of the rupture in the Lakki Plain in November 2001 (detailed accounts of this rupture are given in the Discussion and Fig. 10), thus simplifying the modelling assumptions. Note that the overall deformational pattern between 2001 and 2002 does not change significantly (Fig. 4e, f).

The forward Mogi model was applied to calculate the relative displacements of our control points for two hypothetical point sources at varying depths and locations—one near the centre of Nisyros Island and another one offshore just ESE of Yali. The location of these sources was primarily determined by the observed pattern of deformation, as well as geological and geophysical constraints as previously mentioned. A trial-and-error procedure was adopted to define the best-fit location, depth and source strength parameter of the point sources. Applying the same methodology as

Table 1 Modelling parameters for assumed motion along F1 and F2 faults

Fault system (Fig. 2)	Strike (a) (deg CW N)	Depth (*d*) (km)	Dip (δ) (deg)	Length (L) (km)	U₁[a] (mm)	U₂[a] (mm)	U₃[a] (mm)
F1	222.0	0.6 to 2.0	80.0	3.4 to 8.0	80 to 160	−150 to −260	70 to 110
Best fit model		1.0		4.5	130	−200	100
F2	318.0	0.6 to 2.0	80.0	3.4 to 8.0	70 to 150	−150 to −260	80 to 140
Best fit model		1.0		3.6	100	180	120

[a]U1, U2, U3 are the Left-lateral, Up-dip and Tensile components of the slip vector on the fault plane, respectively

Fig. 6 (**a**) Observed (*black arrows*) and calculated (*red arrows*) horizontal displacements deduced from DGPS measurements for period 1997-2001. Calculated (*red*) arrows result from the combination of two Mogi sources (in-land and off-shore) and fault (*red line*) forward modelling. (**b**) Same as (**a**) but for vertical displacements
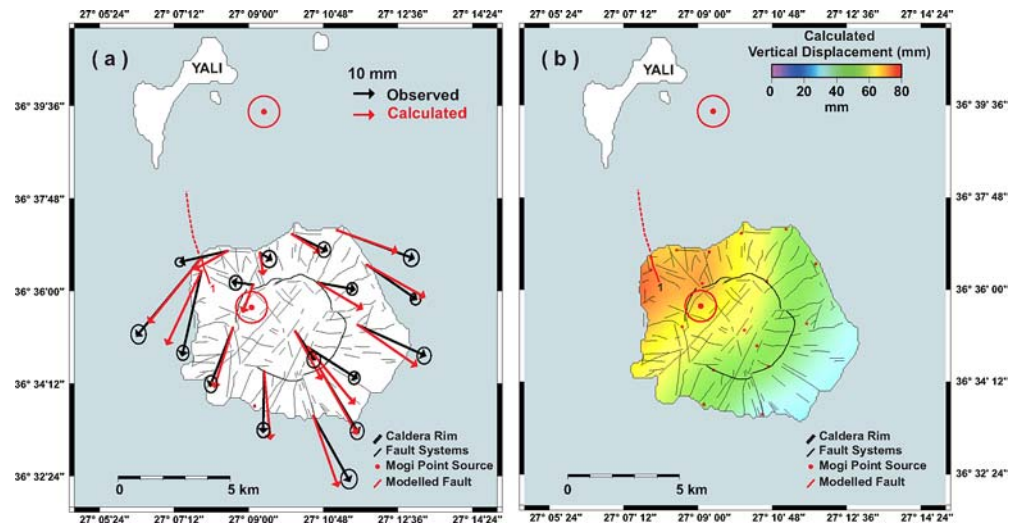
Sigmundsson ([1995]), the residuals of the observed and predicted relative displacements (vertical and horizontal) were determined by least-squares minimization at varying values of depth and radius of the sphere associated with the source strength parameter.

The best fit of the onshore source is located at coordinates [36° 35′ 40.99210″ N, 27° 09′ 04.10122′ E] in WGS'84 datum, or [4054250±500 m N, 781750±500 m E] in the Hellenic datum HGRS'87 (Fig. 6) at a depth of 5500±500 m, and $\Delta V = (7.0 \pm 1.3) \times 10^6$ m^3. The coordinates of the offshore source were determined as [36° 39′ 48.67397″ N, 27° 09′ 22.25204″ E] in WGS'84 datum, or [4061900±500 m N, 781950±500 m E] in HGRS'87 at a depth of 6500±500 m, and $\Delta V = (11.5 \pm 1.7) \times 10^6$ m^3.

The deformational modelling of the NW part of the island was performed by taking into account the observed displacements along the fault passing through Mandraki which was activated during the 1996 seismic crisis, and assuming that displacement along this particular fault occurred also after that period. Active slip along this fault influences both the direction and amplitudes of the observed displacements The combined modelling result including the two Mogi sources and displacement along the Mandraki Fault is depicted in Fig. 6. The relevant modelling parameters are shown in Table 2.

The observed uplift of 30 to 150 mm for the period 1997 to 2001 (Fig. 4e) is consistent with the synthetic data (35 to 80 mm) with the exception of the NW part of the island (Fig. 6b). There, the modelled values of uplift cannot fully account for the observed values recorded in this area. This misfit may be explained by geological constraints of this area. The oldest volcanic rocks are exposed on the uplifted part of the Mandraki Fault, which has a submarine con-

tinuation to at least Yali Island and is clearly identified by detailed multi-beam soundings (Nomikou and Papanikolaou [2000a], [b]; Papanikolaou and Nomikou [2001]). This long-standing zone of crustal weakness was reactivated in the late 1800s (Gorceix [1873c]) and on the basis of fossil evidence its uplifted section is moving faster than the rest of the island (Stiros [2000]).

DInSAR analysis

DInSAR analysis was performed to study the regional deformation on Nisyros Island in conjunction with the DGPS observations that were used as a control on the interferograms. Suitable interferometric pairs of SAR images were selected to produce the DInSAR images (Table 3). Although eight pairs were initially selected, only four are presented because of technical problems with some of the images, together with satellite (ERS-2) orbital problems that were announced by the European Space Agency since February 2001.

The "two-pass differential interferometric method" or "DEM-elimination method" was chosen, using two SAR images to produce one interferogram. A second interferogram had to be created or synthesised to perform the differential analysis. The synthesized interferogram was generated from an existing digital elevation model (DEM) with pixel size of 2 m (Vassilopoulou et al. [2002]), and subsequently subtracted from the original interferogram. After removing all fringes relating to ground elevation only the fringes representing surface displacements remained. Orbital and topographic phase residuals were removed from the raw differential interferogram by mainly adjusting the

Table 2 Parameters of Mandraki fault dislocation for the estimation of ground deformation

Fault No (Fig. 6)	Strike (a) (deg CW N)	Depth d (km)	Dip δ (deg)	U_1^a (mm)	U_2^a (mm)	U_3^a (mm)	Length (km)	Width (km)
1	330.0	0.591	80.0	−35	−15	−12.5	4.0	0.6

[a]U_1, U_2, U_3 are the Left-lateral, Up-dip and Tensile components of the slip vector on the fault plane, respectively

Table 3 DInSAR Pairs of Nisyros Island

Date	Orbit	Frame	Pass	Satellite	Interval (days)	Bp[a] (m)
22-May-1995	20135	2871	descending	ERS-1	245	85
22-Jan-1996	23642	2871	descending	ERS-1		
↕ 4 months overlapping						
04-Sep-1995	21638	2871	descending	ERS-1	351	58
20-Aug-1996	6975	2871	descending	ERS-2		
↕ 2 months overlapping						
11-Jun-1996	5973	2871	descending	ERS-2	1120	44
06-Jul-1999	22005	2871	descending	ERS-2		
↕ 5 months gap						
05-Dec-1999	24188	729	ascending	ERS-2	280	104
10-Sep-2000	28196	729	ascending	ERS-2		

[a]Bp is the perpendicular baseline length

perpendicular baseline line component and yaw angle. The phase differences which then show up as fringes in the final differential interferogram are the result of a range of changes of any displaced point on the ground from one interferogram to the next or, in some cases, of atmospheric path effects. The detailed procedure for DInSAR processing of the Nisyros data is described elsewhere (Parcharidis and Lagios 2001).

Coherence is the parameter that characterizes the quality of the interferogram; the coherence map of the island for each interferometric pair is presented in Fig. 7a. The brighter areas represent good coherence zones, the grey areas fairly good coherence, and finally the darker areas low coherence. The SE and SW part of the island has a good coherence while the northern part and most of the caldera show low coherence, thus indicating loss of information within these zones and consequently unreliable results are expected. This low coherence is attributed to more vegetation and cultivation in the northern part, steep slopes of the caldera rim, and cultivation within the flat part of the caldera. In addition, variations in surface geology may have an influence with the southern part which consists of andesitic and dacitic lava domes, whereas the northern part is mainly covered by unconsolidated pyroclastic material (Fig. 7b). Comparison with the rock classification map indicates good matches between areas of high and low coherence with lavas and pyroclastic successions, respectively.

Each fringe of deformation is directly related to the radar's wavelength, which is 56 mm for the ERS satellites, and represents a line of sight displacement relative to the satellite of only half the above wavelength (i.e. 28 mm). Relative uplift is expressed in each fringe by the colour sequence of Red-Blue-Green (RBG). For subsidence, i.e. motion of the ground surface away from the satellite, the colour sequence for each fringe is GBR. These colour sequences need to be considered whenever the sense of the ground motion is desired.

The differential interferogram for the period May 22, 1995 to January 22, 1996 essentially represents conditions before the start of the seismic crisis (Fig. 8a). Two fringes are recognized indicating an uplift of 56 mm (2×28 mm, i.e. sense of motion of the ground surface is towards the satellite). The inner fringe with an almost circular shape

Fig. 7 (**a**) DInSAR coherence image of Nisyros Island for four interferometric pairs for the period 1995–2000. The "high" and "low" coherence values are represented by brighter and darker areas, respectively. (**b**) Rock classification map of Nisyros Island. Pyroclastic rocks are covering most of the northern part of the island. Lavas are the dominant formations at the central and south-western part
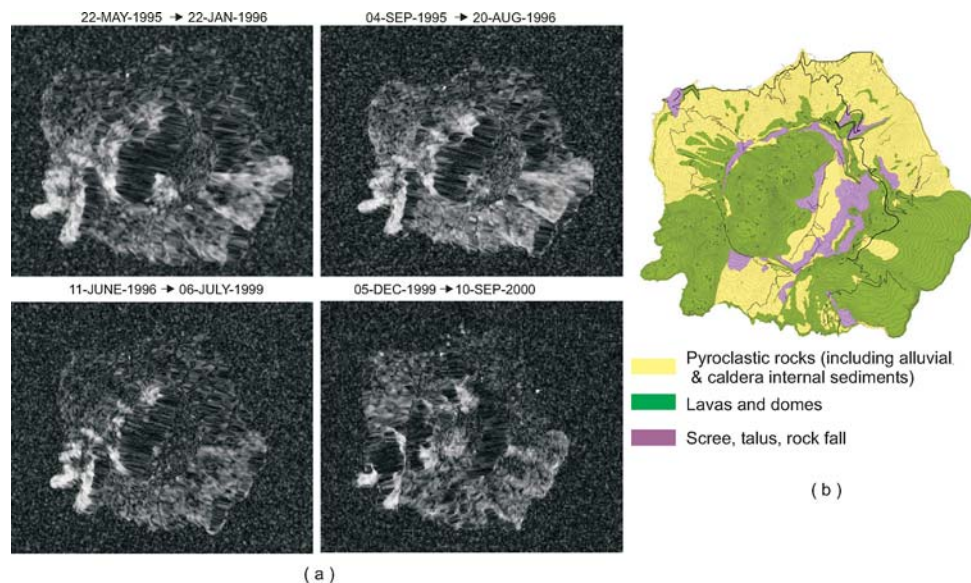
Fig. 8 DInSAR Image of Nisyros Island (magnitude and phase) for the periods: (**a**) May 22, 1995 to January 22, 1996. (**b**) September 4, 1995 to August 20, 1996. (**c**) June 11, 1996 to July 6, 1999. (**d**) December 5, 1999 to September 10, 2000. One fringe of deformation (28 mm) along the line of sight is represented by the sequence of three colours (RGB) indicating relative uplift (RGB)(+) or subsidence (BGR)(−). The shape of the fringes is outlined in the upper right corner
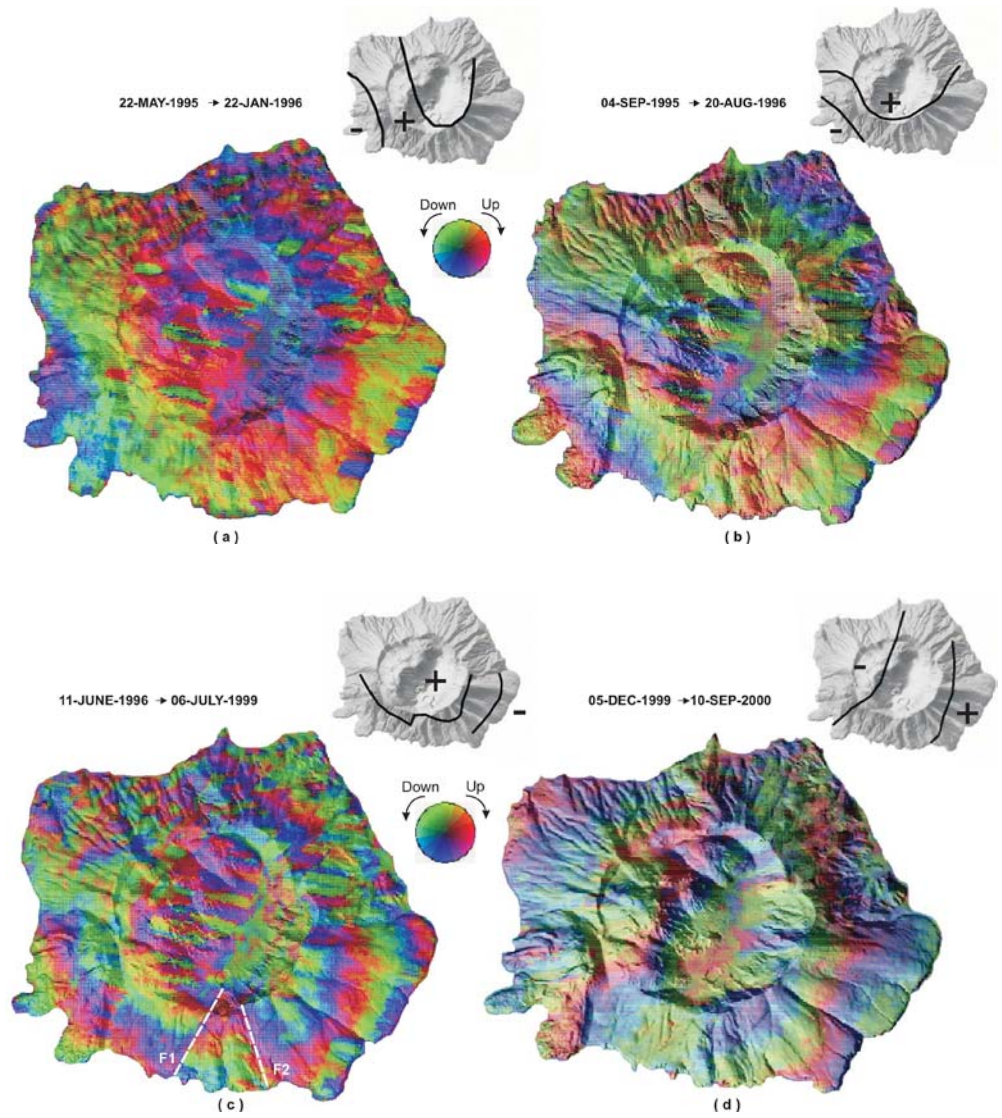
covers a large part of the island, extending from the NW to the southern part but dying out in the NE part (due to poor coherence). The outer second fringe is located on the WSW extremity of the island.

The differential interferogram for the period September 4, 1995 to August 20, 1996 (Fig. 8b) overlaps four months with the previously one. The time span includes most of the intense seismic activity that started in early 1996. Two fringes (2×28 mm = 56 mm of ground motion along the line of sight) are recognized covering the southern half of the island. The inner fringe starts from the western part, continues along the southern caldera rim and terminates at the eastern part. The second outer fringe can be traced in the SW and SE parts of the island. The sense of ground motion is similar to the previous interferogram.

The differential interferogram for the period June 11, 1996 to July 6, 1999 (Fig. 8c) was produced even though the time separation is rather large (more than 3 years). Two fringes (56 mm) indicating uplift along the slant range on the southern half of the island are noted. Considering

the inner fringe, a distinctive characteristic appears in its southern part where an offset to the north is evident that may coincide with crossing of a segment of the F1 fault system (Fig. 2).

The last differential interferogram covers the period December 5, 1999 to September 10, 2000 (Fig. 8d) and is of ascending orbit, while the previous were descending. Two fringes with an almost linear shape and direction NNE-SSW are identified that cover almost all the island. The sense of the ground motion is away from the satellite indicating subsidence change along the slant range of 56 mm.

DInSAR modelling

Interpretation of the observed deformation from the DInSAR analysis was based on a simple Mogi model. A synthetic interferogram for the Nisyros-Yali area was created (Fig. 9) in a descending pass geometry using the forward algorithm of Feigl and Dupre (1999) and propagating the

Fig. 9 Synthetic interferometric image of the Nisyros-Yali area deduced from two Mogi point sources: One located below Nisyros and the other off-shore north of Nisyros
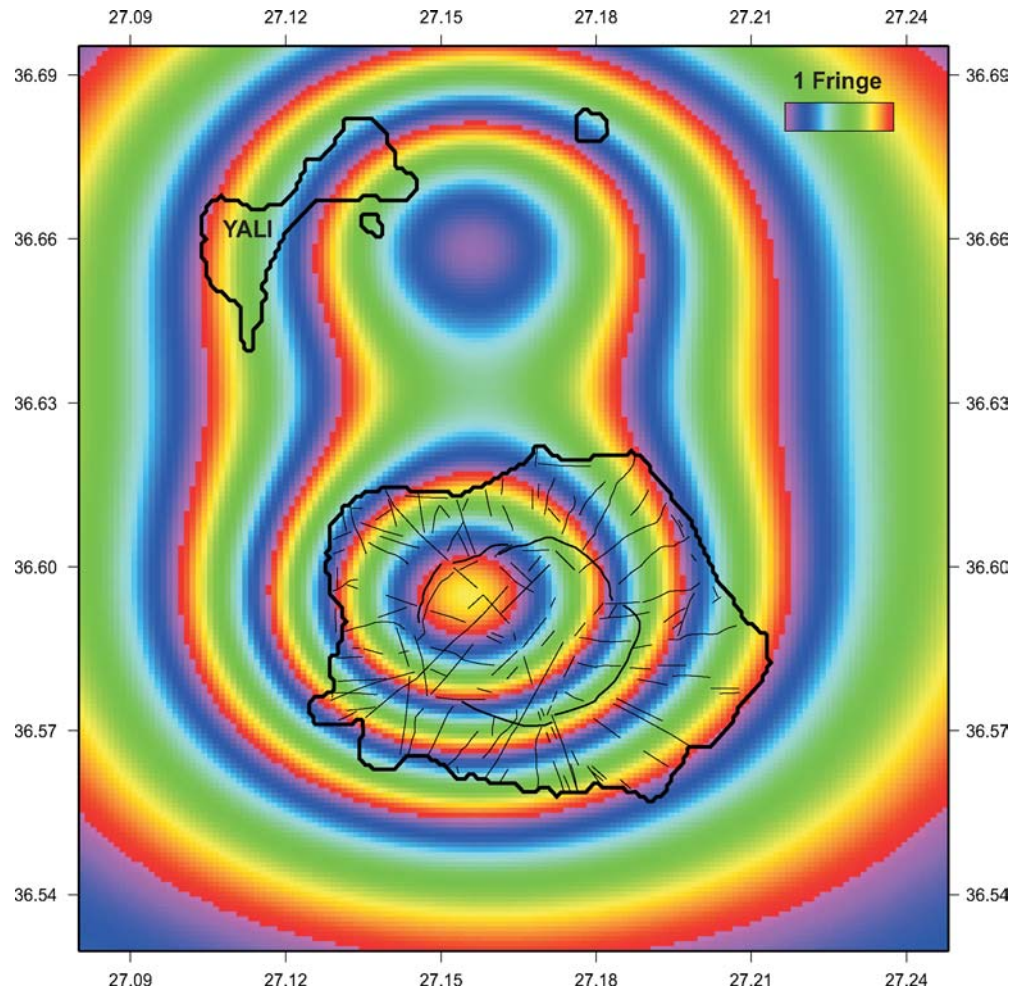
two Mogi source locations as determined by the DGPS modelling. The observed interferogram corresponding to the longest period 1996 to 1999 (Fig. 8c) was chosen for comparison to the synthetic data that are presented in Fig. 9.

The "figure-eight" pattern of the fringes in the synthetic interferogram is the result of two Mogi sources of different strength and depth. The presence of the second offshore source results in the opening of the fringes over Nisyros as compared to the expected circular fringes that would be generated by only one source located onshore. The number, the shape and the location of the synthetic fringes in the southern part are in a good agreement to the observed differential interferogram (Fig. 8c) in the SE part (2 fringes). In the SW part (1 fringe) the modelled fringe intersects the coast whereas the observed fringe does not. Low coherence in the observed data for the northern part of the island prevents comparison with modelled results. The maximum amplitude of ground deformation deduced from the synthetic modelling along the line of sight is about 133 mm which, if projected onto the direction along the slant range, is close to maximum deformation as determined by DGPS analysis ($\approx$120 mm) for the period 1997 to 2000.

Results from the present modelling are consistent with previously published work (Sykioti et al. 2003) with respect to the shape of the interferometric fringes especially

in the SE part of the island. However, only one Mogi source with an offset of about 1 km NW relative to our onshore source was considered in that study. Their modelled DInSAR images correspond to the period 1995 to 1997, but overlap by only one year with our data. The incorporation of a second source in the present study is warranted by the results obtained from DGPS modelling.

Discussion and conclusions

Two separate scenarios to explain the observed deformation on Nisyros have been considered in this study. The first assumes movement along the major F1 and F2 fault zones and the second the inflation/deflation of magma chambers combined with movement along the Mandraki Fault. DGPS and DInSAR modelling yields better results for the latter scenario and suggests that a combination of mechanisms involving Mogi point sources and fault movement has produced the observed deformation. In general, a similar combination of mechanisms can be invoked to account for deformation in the broader region that is consistent with the observed seismicity which is of tectonic and volcanic origin.

We note that for the first scenario, suitable fits were obtained from DGPS modelling for only a few control points. For the second scenario, better qualities of fits were obtained for both components for almost all of the control points. However, along the NW edge of the island there is a deviation in the vertical component that cannot be explained by either modelling scenario. An anomalous uplift pattern of this area has been noted previously (Di Paola 1974; Stiros 2000).

DInSAR analysis indicates that uplift (of the order of 56 mm along the slant range) occurred on Nisyros during 1995. Comparison of the differential interferogram of May 22, 1995 to January 22, 1996 with previously published work (Sachpazi et al. 2002; Sykioti et al. 2003) shows one additional fringe of deformation in the latter, but this is tentatively attributed to its longer period that extended 4 months into 1996. We therefore conclude that the deformation on Nisyros had already started prior to the seismic crisis in early 1996.

In the following period, 1996 to 1999, the ground surface uplifted, which is consistent with the deformational pattern observed by the DGPS measurements that started in June 1997. However, the pattern changed from uplift to subsidence in 2000 (Fig. 8d), and the shape of the fringes from sub-circular to almost linear. This linearity is not fully supported by the DGPS observations (Fig. 5d) of the same period. The surface subsidence that was observed in the NW part and the small uplift in the SE part (Fig. 5d) might have led to the linear generation of the fringes as controlled by the presence of the F1 fault zone (Fig. 2) that is oriented parallel to the direction of fringes.

The deformational pattern after 2000 is based only on DGPS observations and does not change significantly. We therefore conclude that Nisyros has uplifted since at least 1997. The surface deformation is of the order of a few centimeters to a decimeter, and has been modelled by two sources of dilatation at depths of 5500 and 6500 m.

The lakki plain rupture

A large irregular rupture 1 to 5 m wide at the surface and narrowing downwards to a depth of about 10 m opened overnight without any precursory phenomena on November 20, 2001 in the central part of the Lakki Plain (Fig. 10). It had a length of approximately 350 m and was oriented in an almost N-S direction. One year later (December 18, 2002), the rupture extended southwards for another 250 m with smaller perpendicular offsets. The rupture showed neither signs of vertical displacement nor indications of deeper penetration through the young, up to 150 m-thick, epiclastic and hydrothermal caldera deposits (Geothermica Italiana 1983, 1984). Therefore, only horizontal tensional forces could have caused the instant generation of such a rupture in the uppermost surface layer of consolidated soft sediments. In this respect, the observed horizontal displacements during the period 1997 to 2001 have been attributed mainly to bulging at deeper levels that led to uncompensated stress conditions in the near surface. The sudden rup-
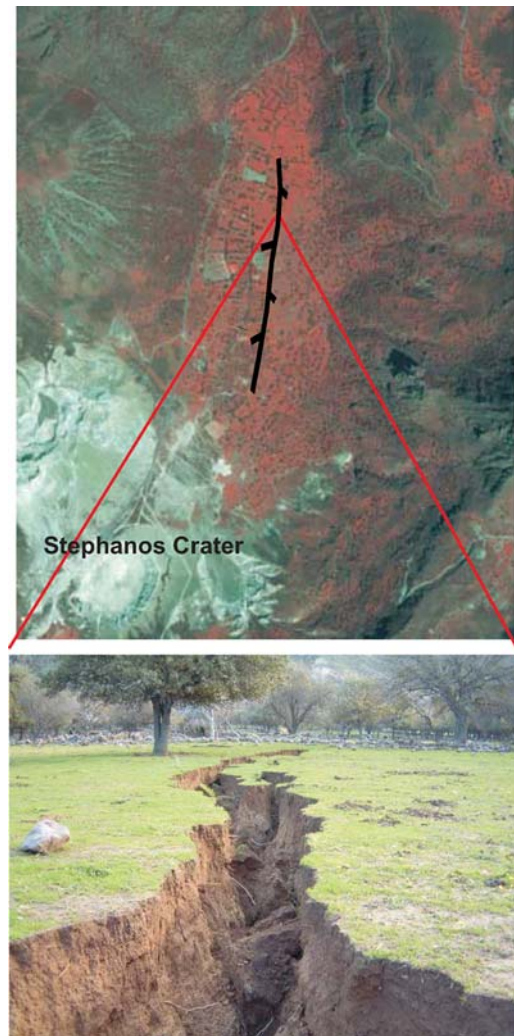
Fig. 10 The 600 m long rupture formed in the Lakki Plain (see rectangle in Fig. 2) in 2001 and 2002 superimposed on an IKONOS-2 ortho-image

turing can be explained by stress release without producing any seismic signature.

The approximate N-S orientation of the rupture is almost parallel to the F4 fault system and to the observed DInSAR fringes for the period 1999 to 2000 (Fig. 8d) and seems to be apparently consistent with E-W extension. However, the differential interferogram for 2000 indicates opposite deformation to the previous pattern, suggesting deflation and hence a tendency to relieve any surface extensional bending. The deformational pattern though changed again during the next two years when the rupture actually manifested and its length extended. Relative uplift was observed in 2001 with respect to 2000 (Fig. 5e), while in 2002, further uplift at the center of the island took place, while subsidence occurred at the eastern part (Fig. 5f).

The mandraki fault

Finally, we would like to emphasise the importance of the Mandraki Fault (with its clear sub-marine northward con-

13

tinuation) on the local tectonic regime. This fault has been active since the late 19th century and vertical displacement along this zone, which may extend deep into the crust, is the largest on Nisyros. It would not be surprising if future tectonic, magmatic and hydrothermal activity started along this weak zone.

Acknowledgments This work was supported by GEOWARN EU Project (IST-1999-12310) and *KAPODISTRIAS* of the Special Account for Research Grants of the National and Kapodistrian University of Athens. We would like to thank Dr. B. Damiata, Prof. D. Papanikolaou, Dr. F. Sigmundsson and Dr. G. Stavrakakis for their help and support. Also, Dr. Sp. Vassilopoulou, Dr. R. Gogu and Mr. B. Jenny who generated the DTM model, the GIS structural and geotechnical maps of Nisyros Island. Many thanks are also extended to Dr. J. Alexopoulos, Mr. S. Chailas & Mr. L. Tzannetos for their fieldwork assistance. This paper benefited significantly from constructive comments by Prof. Geoff Wadge and an anonymous reviewer.

References

Allen SR, Stadelbauer E, Keller J (1999) Stratigraphy of the Kos Plateau Tuff: Product of a major Quaternary explosive rhyolitic eruption in the Eastern Aegean, Greece. Int J Earth Sci 88:132–156

Brombach T, Cardellini C, Chiodini G, Hunziker JC, Marini L (2001) Soil degassing and thermal energy fluxes from the southern Lakki Plain, Nisyros (Greece). Geophys Res Lett 28:69–72

Brombach T, Caliro S, Chiodini G, Fiebig J, Hunziker JC and Raco B (2003) Geochemical evidence for mixing of magmatic fluids with seawater, Nisyros hydrothermal system, Greece. Bull Volcanol 65:505–516

Chiodini G, Cioni R, Leonis C, Marini L, Raco B (1993) Fluid geochemistry of Nisyros Island, Dodecanese, Greece, J. Volcanol Geotherm Res 56:95–112

Chiodini G, Brombach T, Caliro S, Cardellini C, Marini L, Dietrich V (2002) Geochemical indicators of possible ongoing volcanic unrest at Nisyros Island (Greece). Geophys Res Let 29(16) 10.1029/2001gl014355

Dawes GJK, Lagios E (1991) A Magnetotelluric Survey of the Nissyros Geothermal Field (Greece). Geothermics 20(4):225–235

Di Paola GM (1974) Volcanology and petrology of Nisyros Island (Dodecanese, Greece). Bull Volcanol 38:944–987.

Dixon TH (1991) An introduction to the Global Positioning System and some geological applications. Rev Geophys 29:249–276

Feigl K, Dupre E (1999). RNGCHN: A program to calculate displacement components from dislocations in elastic half-space with applications for modelling geodetic measurements of crustal deformation. Comput Geosci 25(6):695–704

Fytikas M, Guiliani O, Innocenti F, Marinelli G, Mazzuoli R (1976). Geo-chronological data on recent magmatism of the Aegean Sea. Tectonophysics 31:29–34

Fytikas M, Innocenti F, Manetti P, Mazuoli R, Peccerilo A, Villari L(1984). Tertiary to Quaternary evolution of the volcanism in the Aegean Region. In: Dixon JE, Robertson AHF (ed) The Geological Evolution of the Eastern Mediterranean. Geol Soc London Spec Pub. 17: 687–699

Geothermica Italiana.(1983) Nisyros 1 geothermal well. PPC-EEC report:1–106

Geotermica Italiana. (1984) Nisyros 2 geothermal well. PPC-EEC report, 1–44

Gorceix MH (1873a) Sur d'état du volcan de Nisyros au mois de mars 1873. CR Acad Sci (Paris) 77:597–601

Gorceix MH (1873b) Sur la récente éruption de Nisyros. CR Acad Sci Paris 77:1039

Gorceix MH (1873c) Sur l'éruption boueuse de Nisyros. CR Acad Sci Paris 77:1474–1477

Hardimann JC (1999) Deep sea tephra from Nisyros Island, Eastern Aegean Sea, Greece. In: Firth CR, McGuire WJ (eds) Volcanoes in the quaternary. Geol Soc (London), Spec Publ 161 69–88

Ioannidis K (1998) Nisyros Island: Observed damages to buildings in Mandraki. Newslett, Eur Center Prevent Forecastf Earthquak 2 33–35

Jackson J (1994) Active tectonics of the Aegean region. Ann Rev Earth Planet Sci 22: 239–271

Kavouridis T, Kuris D, Leonis C, Liberopoulou V, Leontiadis J, Panichi C, La Ruffa G, Caprai A (1999) Isotope and chemical studies for a geothermal assessment of the island of Nisyros (Greece). Geothermics 28:219–239

Keller J (1969) Origin of rhyolites by anatectic melting of granite and crustal rocks. The example of rhyolitic pumice from the island of Kos (Aegean Sea). Bull Volcanol 33:942–959

Keller L, Rehren Th, Stadlbauer E (1990) Explosive volcanism in the Hellenic Arc; a summary and review. In: DA Hardy, J Keller, VP Galanopoulos, NC Flemming, TH Druitt (eds) Thera and the Aegean World III. Proc 3rd International Congress The Thera Foundation, London 2: 13–26

Lagios E (1991) Magnetotelluric study of the structure of the Nisyros Geothermal Field. Bull Geol Soc Greece 25(3):393–407

Lagios E, Chailas S, Giannopoulos J, Sotiropoulos P (1998) Surveillance of Nisyros Volcano: Establishment and remeasurement of GPS and Radon Networks. Bull Geol Soc Greece 32(4):215–227

Lagios E. (2000) Intense crustal deformation rates on Nisyros Island (Greece), deduced from GPS studies, may foreshadow a forthcoming volcanic event. In: S Balassanian et al (ed) Proc. 2nd Intern. Conf. On Earthquake Hazard and Seismic Risk Reduction, Kluwer Academic Publishers, pp 249–259

Le Pichon X, Angelier J (1979) The Hellenic arc and trench system: a key to the evolution of the Eastern Mediterranean. Tectonophysics 60:1–42

Limburg EM, Varekamp JC (1991) Young pumice deposits on Nisyros, Greece. Bull Volcanol 54(1):68–77

McTigue DF (1987) Elastic stress deformation near a finite spherical magma body: Resolution of the point source paradox. J Geophys Res 92(B12):12931–12940

Makris J, Chonia T (1999) Active and Passive Seismic studies of Nisyros Volcano, East Aegean Sea. Proc. 1999 CCSS Workshop held in Dublin, Ireland. "Active and Passive Seismic Techniques Reviewed", In: AW Brian, Jacob Chr J Bean, Stephen, TF Jacob (eds), pp 9–12

Makris J, Stobbe T (1984) Physical properties and state of the crust and upper mantle of the Eastern Mediterranean Sea deduced from geophysical data. Marine Geol 55: 347–363.

Makropoulos K, Drakopoulos J, Latoussakis J (1989) A revised earthquake catalogue for Greece since 1900. Publ. No 2. Geophys J Int 98:391–394

Marini L, Principe C, Chiodini G, Cioni R, Fytikas M, Marinelli G (1993) Hydrothermal eruptions of Nisyros (Dodecanese, Greece). Past events and present hazard. J Volcanol Geotherm Res 56:71–95

McKenzie DP (1972) Active tectonics of the Mediterranean Region. Geophys J R Astron Soc 30:109–185

Mogi K (1958) Relations between the eruptions of various volcanoes and the deformations of ground surfaces around them. Bull Earthquake Res Inst Univ Tokyo 36: 99–134

Nomikou P, Papanikolaou D (2000a) Active geodynamics at Nisyros, the eastern edge of the Aegean Volcanic Arc: Emphasis on the submarine survey. Proc.3rd Int. Conf. Geology East. Mediterranean, Sept.1998, pp.97–103

Nomikou P, Papanikolaou D (2000b) Submarine survey of the volcanic centres around Nisyros island using multi beam system and the submersible Thetis. International Earth Sciences Colloquium on the Aegean Region, Izmir, Turkey, Abstracts pp.198

Okada Y (1985) Surface deformation due to shear and tensile faults in a half-space. Bull Seism Soc America 75(4): 1135–1154

Papadopoulos GA, Sachpazi M, Panopoulou G, Stavrakakis G (1998) The volcano-seismic crisis of 1996-97 in Nisyros, SE Aegean Sea, Greece. Terra Nova 10: 151–154

Papanikolaou D, Nomikou P (2001) Tectonic structure and volcanic centres at the eastern edge of the Aegean Volcanic Arc around Nisyros Island. Bull Geol Soc Greece XXXIV:1289–296, Proc. 9th Intern. Congress, Athens, Sept. 2001

Papanikolaou D (1993) Geotectonic evolution of the Aegean. Bull Geol Soc Greece 18(1): 33–48

Papanikolaou D, Lekkas E, Sakelariou DT (1991) Geological structure and evolution of Nisyros Volcano. Bull Geol Soc Greece 25(1):405–419

Parcharidis I, Lagios E (2001) Deformation in Nisyros Volcano (Greece) using Differential Radar Interferometry. Bull Geol Soc Greece 34(4):1587–1594

Pe-Piper G, Piper DJW (2002) The Igneous Rocks of Greece. The anatomy of an orogen. Gebr. Bornträger, Berlin, Stuttgart, pp 1–573

Rothacher M, Beutler G, Gurtner W, Brockmann E, Mervart L (1993) Bernese GPS Software Documentation version 3.4. Astronomical Institute, University of Berne, Switzerland

Sachpazi M, Kontoes C, Voulgaris N, Laigle M, Vougioukalakis G, Sykioti O, Stavrakakis G, Baskoutas J, Kalogeras J, Lepine JC (2002) Seismological and SAR signature of unrest at Nisyros Caldera, Greece. J Volcanol Geotherm Res 116:19–33

Sigmundsson F (1995) GPS Monitoring of Volcanic Deformation in Iceland. Cahiers du Centre Europeen et de Seismologie 8:79–98.

Sigmundsson F, Einarsson P, Bilham R (1992) Magma chamber deflation recorded by the Global Positioning System: The Hekla 1991 eruption. Geophys Res Lett 19: 1483–1486

SKI Pro (1999) Static Kinematic Software, Version 3.2, LEICA AG, CH-9435 Heerbrugg, Switzerland

Smith AG (1971) Alpine deformation and the oceanic areas of the Tethys, Mediterranean and Atlantic. Bull Geol Soc Am 82: 2039–2070

Smith PE, York D, Chen Y, Evensen NM (1996) Single crystal 40Ar/39Ar dating of a late Quaternary paroxysm on Kos, Greece; concordance of terrestrial and marine ages. Geophys Res Lett 23 (21):3047–3050.

Stiros SC (2000) Fault pattern of Nisyros Island Volcano (Aegean Sea, Greece): Structural, coastal and archaeological evidence. In: McGuire WJ, Griffiths DR, Hancock PL, Stewart IS (eds) The archaeology of Geological Catastrophes. Geological Society, London, Spec. Public.7: 385–397

Stiros SC, Vougioukalakis G (1996) The 1970 Yali (SE edge of the Aegean Volcanic Arc) earthquake swarm: Surface faulting associated with a small earthquake. Ann. Tecton X:20–30.

Sykioti O, Kontoes C, Elias P, Briole P, Sachpazi M, Paradissis D, Kotsis I (2003) Ground deformation at Nisyros Volcano (Greece) detected by ERS-2 SAR differential interferometry. Int J Remote Sens 24:183–188.

Triantaphyllis M (1994) Geological map of Greece, western Kos sheet (Kefalos) 1:50000. Inst. Geology and Mineral Exploration (IGME), Athens, Greece

Triantaphyllis M, Mavrides A (1998) Geological map of Greece, Eastern Kos sheet 1:50000. Inst. Geology and Mineral Exploration (IGME), Athens, Greece.

Vassilopoulou S, Hurni L, Dietrich V, Baltsavias M, Pateraki M, Lagios E, Parcharidis I (2002) Ortho-Photo generation using IKONOS-2 Imagery and high resolution DEM: A case study on monitoring the volcanic hazard on Nisyros Island. ISPRS J Photogramm Remote Sens 57:24–38.

Vougioukalakis G (1993) Volcanic Stratigraphy and Evolution of Nisyros Island. Bull Geol Soc Greece 28 2:239–258.

Zebker H, Goldstein R (1986) Topographic Mapping from Interferometric SAR Observations. J Geophys Res 91(B5):4993–4999.